Supporting information for

# Kinetic Analysis of Nano-structures Formed by Enzyme-Instructed Intracellular Assemblies against Cancer Cells

Jie Li[†], Domenico Bullara[†], Xuewen Du[†], Hongjian He[†], Stavroula Sofou[‡], Ioannis G. Kevrekidis[‡], Irving R. Epstein[*†] and Bing Xu[*†]

[†]Department of Chemistry, Brandeis University, 415 South Street, Waltham, MA 02454, USA

[‡]Department of Chemical and Biomolecular Engineering, Johns Hopkins University, Baltimore, MD 21218, USA

**Contents**

## 1. Materials and equipment

**Materials.** All the reagents were used as received without further purification. N,N-diisopropylethylamine (DIPEA), N,N'-diisopropylcarbodiimide (DIC), O-benzotriazole-N,N,N',N'-tetramethyl-uronium-hexafluoro-phosphate (HBTU), N-hydroxysuccinimide (NHS), and taurine were purchased from ACROS Organics USA. All amino acid derivatives were purchased from GL Biochem (Shanghai) Ltd.

**Instruments.** Products were purified using a Waters Delta600 HPLC system equipped with an XTerra C18 RP column and an in-line diode array UV detector. LC-MS spectra were acquired on a Waters Acquity Ultra Performance LC with Waters MICROMASS detector. TEM images on were taken on a Morgagani 268 transmission electron microscope. Rheology was performed on a TA ARES-G2 rheometer. Proton NMR spectra were collected on a Varian Unity Inova 400 with DMSO as solvent. MTT assay for cell cytotoxicity was carried out on a DTX880 Multimode Detector.

## 2. Synthesis and characterizations

**Scheme S1.** General synthetic route of the precursor (LD-**1**-$SO_3$ as an example).

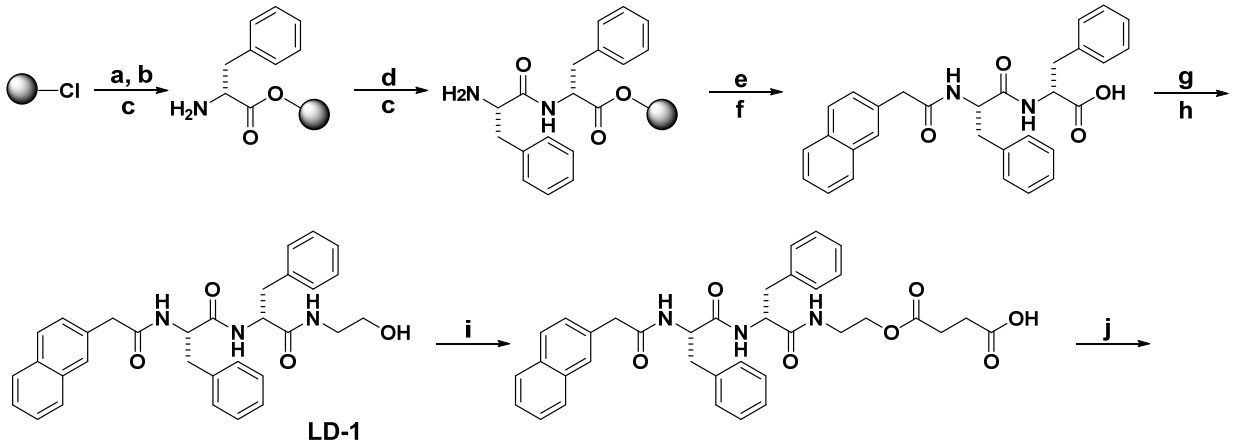


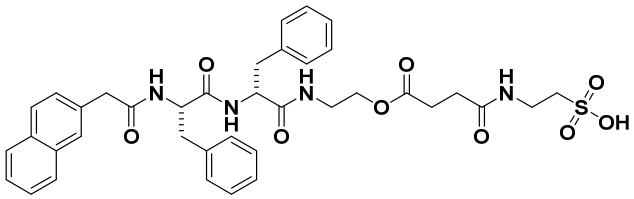


a) Fmoc-L-Phe-(OH), DIEA, DMF, rt, 40 mins; b) Solution of $CH_2Cl_2$: MeOH: DIEA=16:3:1, rt, 10 mins for twice; c) 20% piperdine in DMF, rt, 20 mins; d) Fmoc-D-Phe-(OH), HBTU, DIEA, DMF, rt, 40 mins; e) 2-naphthaleneacetic acid, HBTU, DIEA, DMF, rt, 40 mins; f) 95% TFA in H2O, rt, 2h; g) NHS, DIC, THF, rt, 3-4h; h) ethanolamine, DIEA, THF, rt, 1h; i) succinic anhydride, DIEA, DMF, rt, overnight; j) taurine, HBTU, DIEA, DMF, rt, overnight

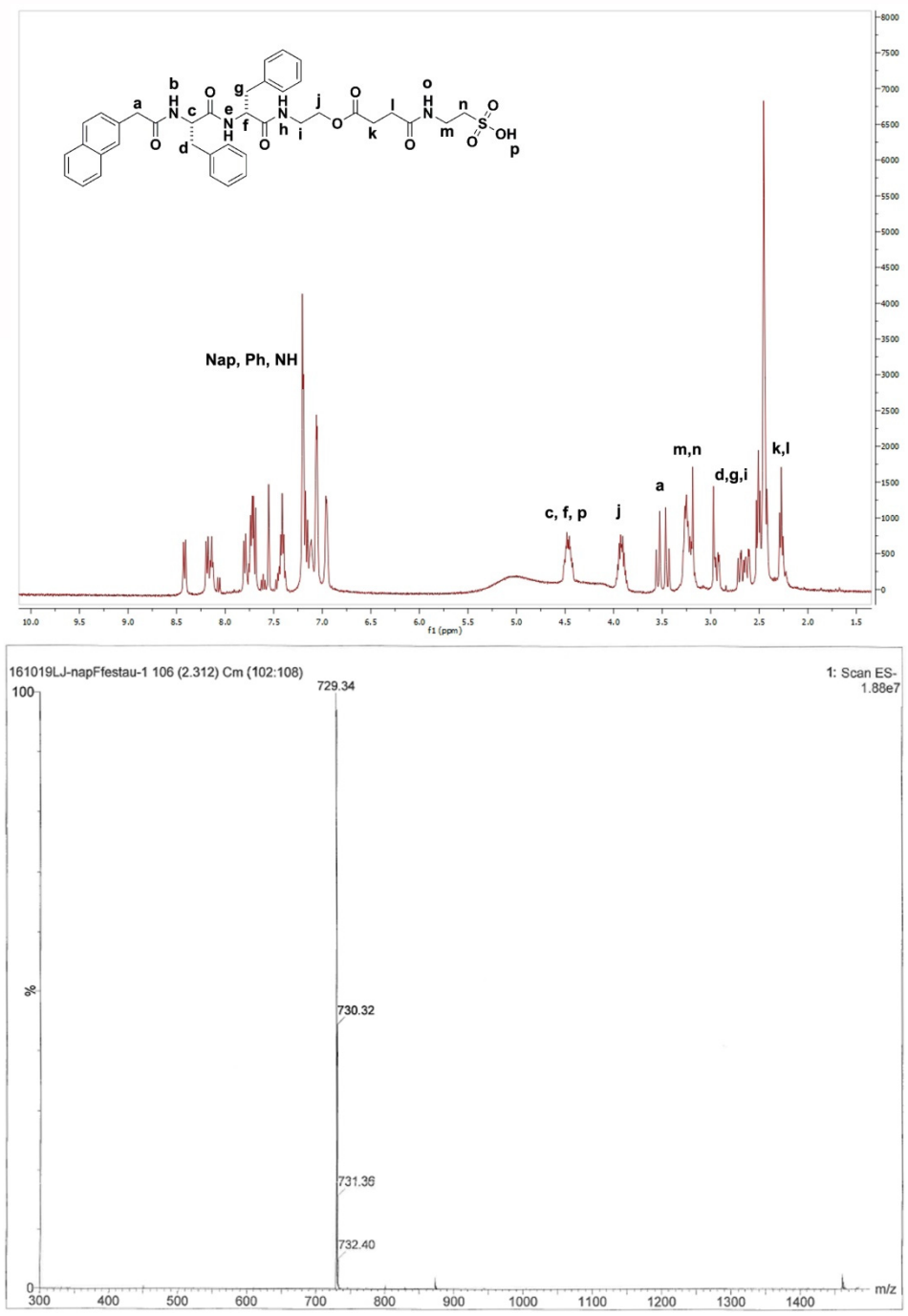


**Figure S1.** $^{1}$H NMR spectrum of LD-**1**-$SO_3$ in DMSO-$d_6$ and its LC-MS spectrum.

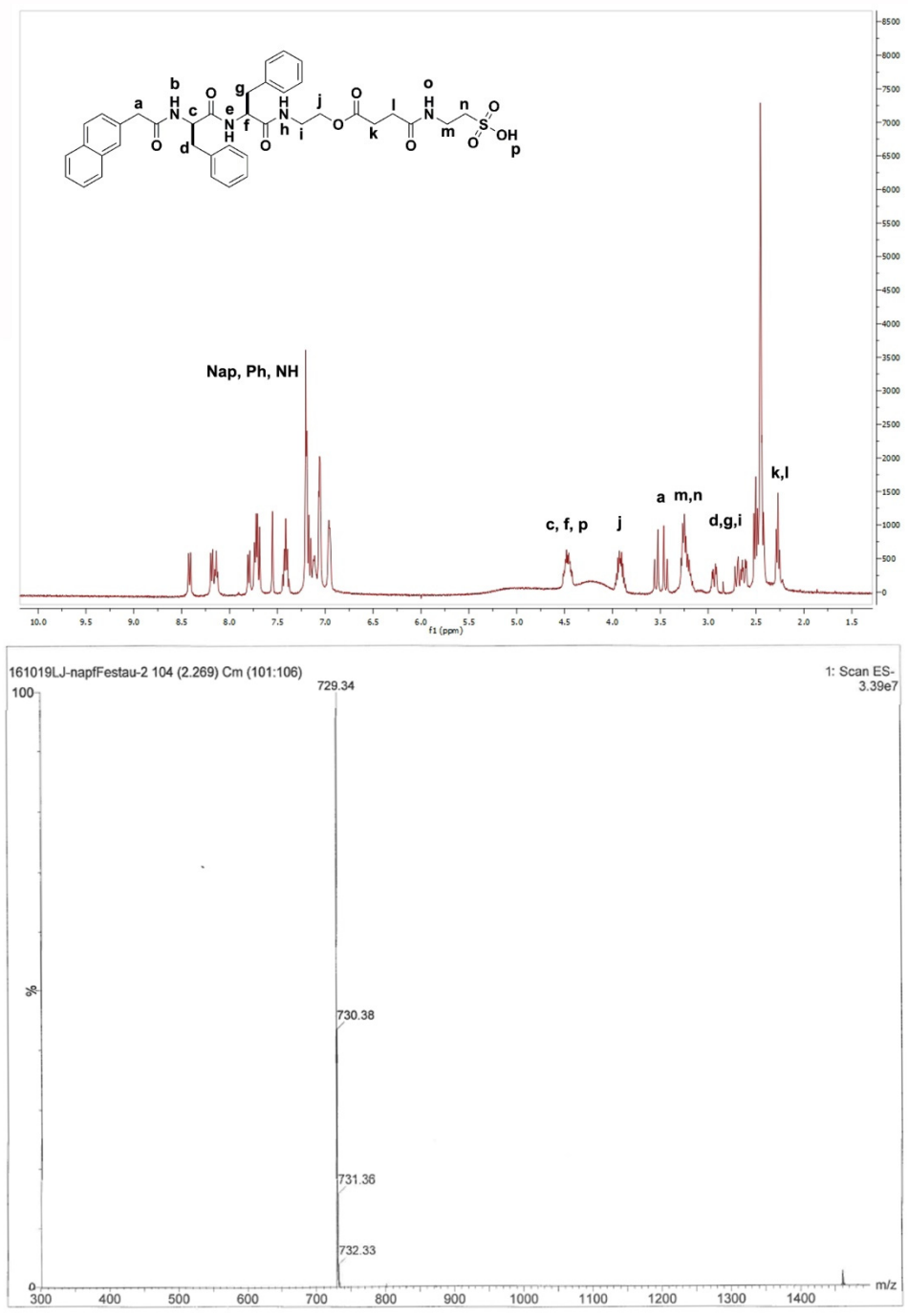


**Figure S2.** $^{1}$H NMR spectrum of DL-**1**-$SO_3$ in DMSO-$d_6$ and its LC-MS spectrum.

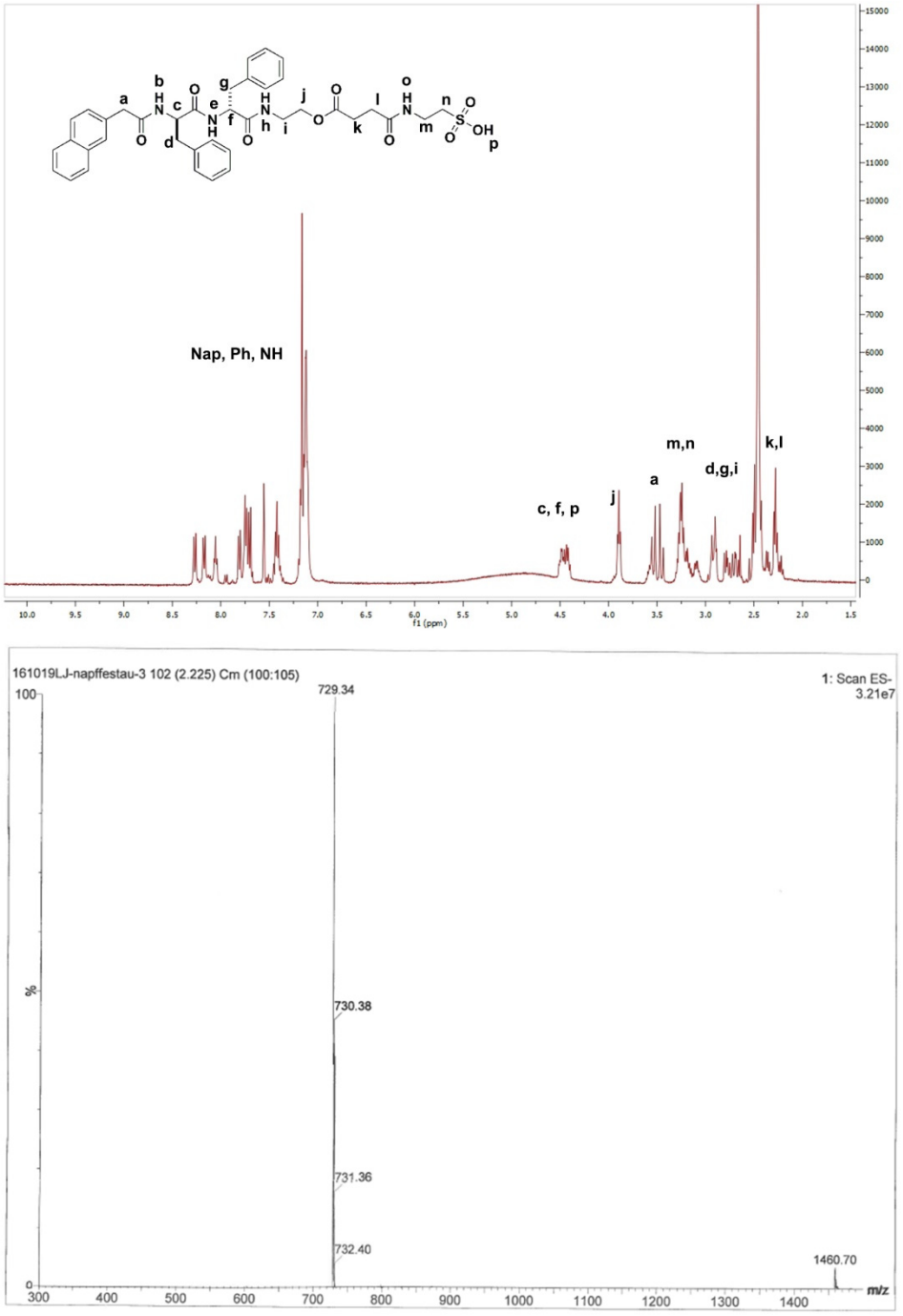


**Figure S3.** $^{1}$H NMR spectrum of DD-**1**-$SO_3$ in DMSO-$d_6$ and its LC-MS spectrum.

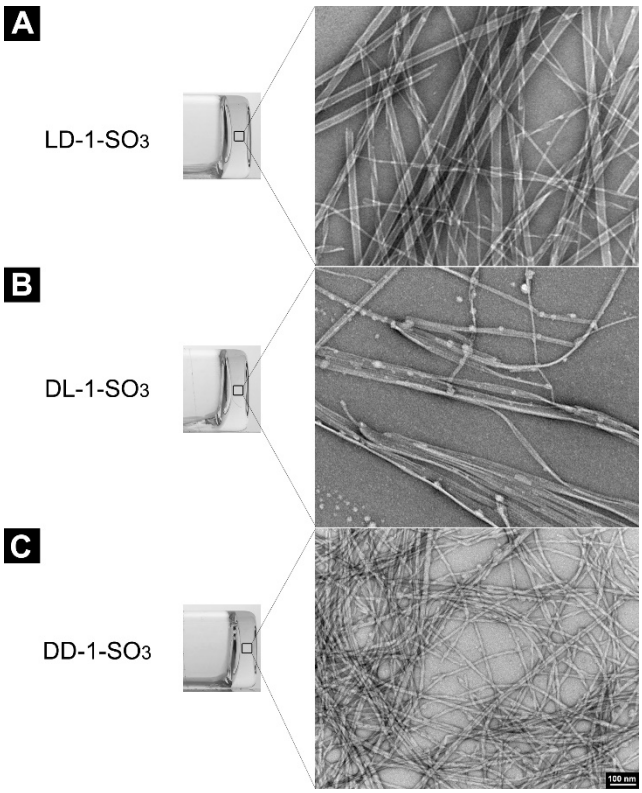


**Figure S4.** Optical and TEM images of hydrogels formed by addition of CES (1 U/mL) to 0.2 wt % solutions of the three precursors in PBS buffer (scale bar = 100 nm).

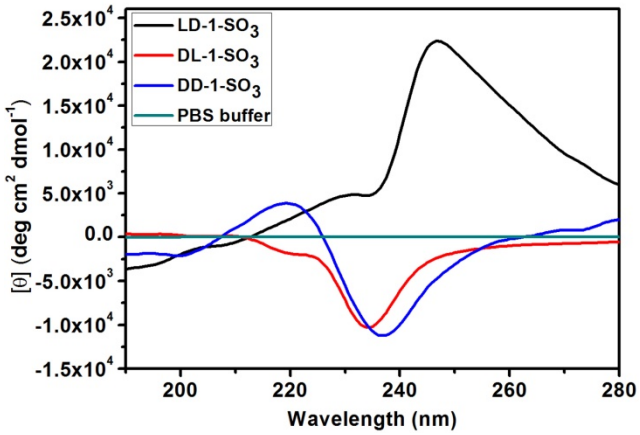


**Figure S5.** Circular dichroism (CD) spectra of 0.2 wt% hydrogels of the precursors LD-**1**-$SO_3$, DL-**1**-$SO_3$ and DD-**1**-$SO_3$ in PBS buffer at pH = 7.4 with addition of CES for 24 h (1 U/mL).

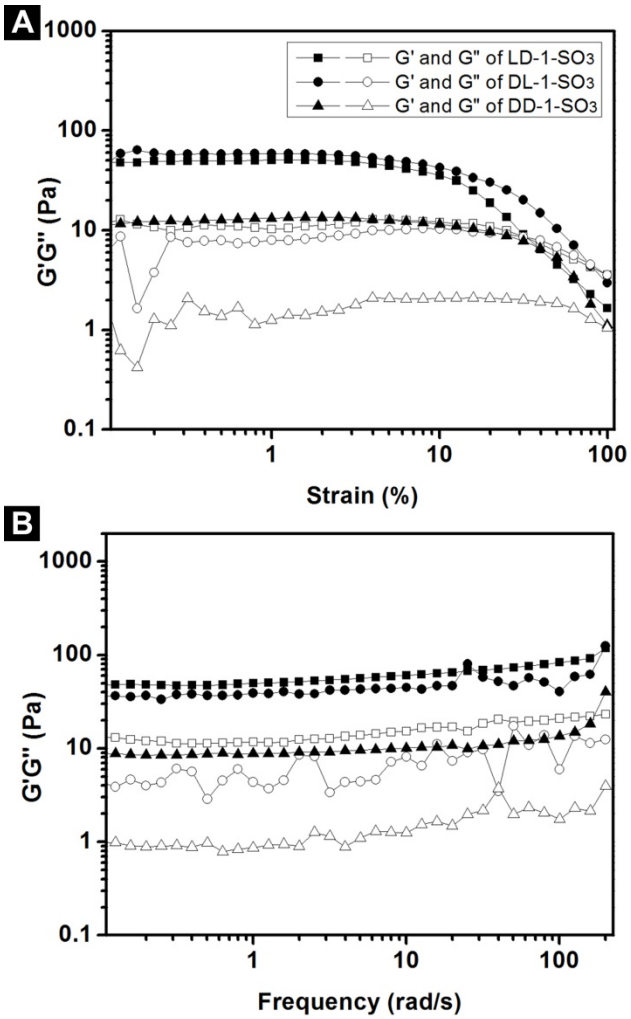


**Figure S6.** (A) Strain and (B) frequency dependence of dynamic storage moduli G' and loss moduli G'' of the gels formed by LD-**1**-$SO_3$, DL-**1**-$SO_3$ and DD-**1**-$SO_3$ at 0.2 wt% upon treatment with 1 U/mL of CES at pH 7.4 in PBS buffer for 24 h.

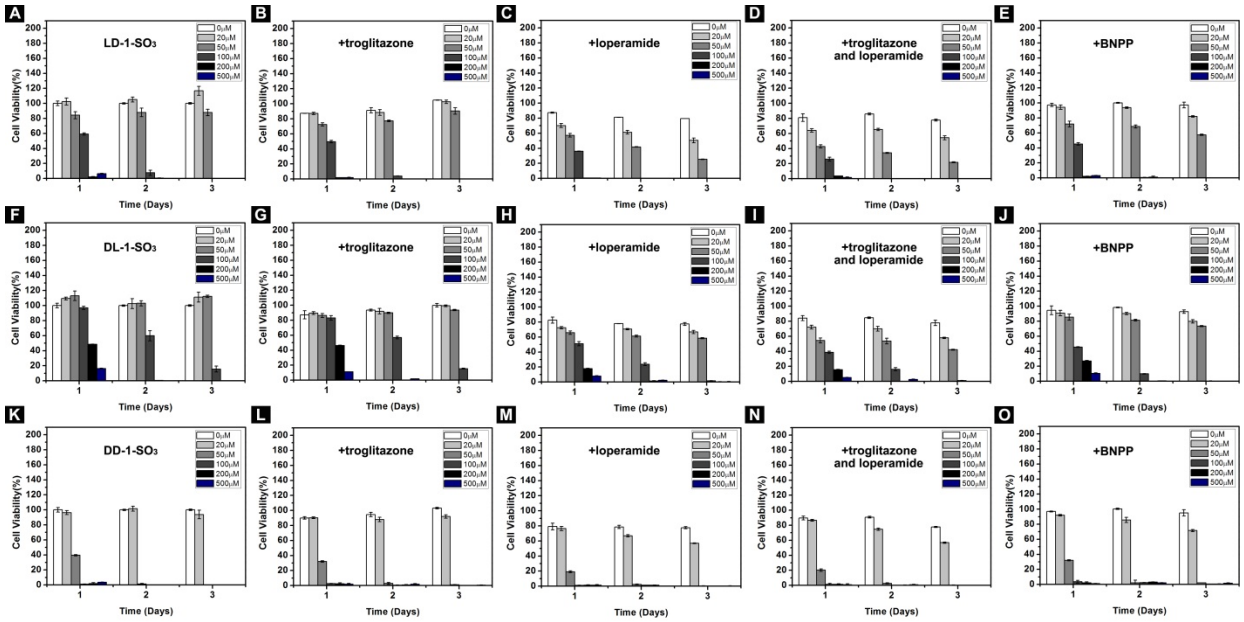


**Figure S7.** Viability of OVSAHO cells after being treated with (A) LD-**1**-$SO_3$; (B) LD-**1**-$SO_3$ with 10 μM troglitazone (CES1 inhibitor); (C) LD-**1**-$SO_3$ with 10 μM loperamide (CES2 inhibitor); (D) LD-**1**-$SO_3$ with 10 μM troglitazone and 10 μM loperamide; (E) LD-**1**-$SO_3$ with 100 μM BNPP (CES inhibitor); (F) DL-**1**-$SO_3$; (G) DL-**1**-$SO_3$ with 10 μM troglitazone; (H) DL-**1**-$SO_3$ with 10 μM loperamide; (I) DL-**1**-$SO_3$ with 10 μM troglitazone and 10 μM loperamide; (J) DL-**1**-$SO_3$ with 100 μM BNPP; (K) DD-**1**-$SO_3$; (L) DD-**1**-$SO_3$ with 10 μM troglitazone; (M) DD-**1**-$SO_3$ with 10 μM loperamide; (N) DD-**1**-$SO_3$ with 10 μM troglitazone and 10 μM loperamide; (O) DD-**1**-$SO_3$ with 100 μM BNPP.

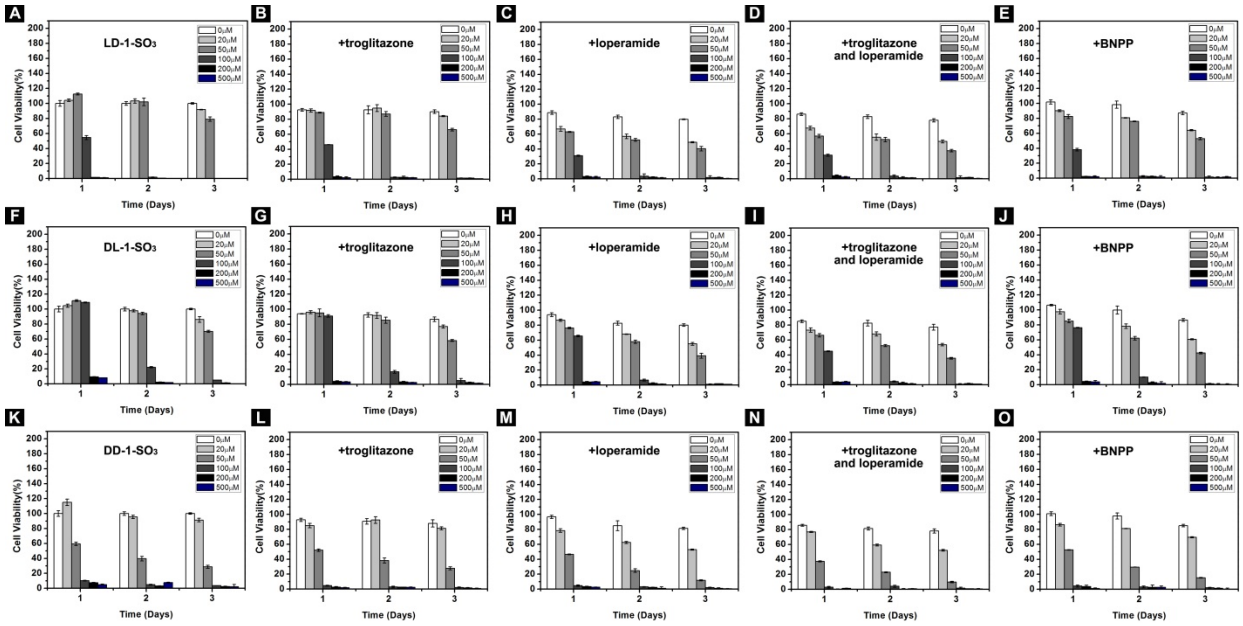


**Figure S8.** Viability of HeLa cells after being treated with (A) LD-**1**-$SO_3$; (B) LD-**1**-$SO_3$ with 10 μM troglitazone (CES1 inhibitor); (C) LD-**1**-$SO_3$ with 10 μM loperamide (CES2 inhibitor); (D) LD-**1**-$SO_3$ with 10 μM troglitazone and 10 μM loperamide; (E) LD-**1**-$SO_3$ with 100 μM BNPP (CES inhibitor); (F) DL-**1**-$SO_3$; (G) DL-**1**-$SO_3$ with 10 μM troglitazone; (H) DL-**1**-$SO_3$ with 10 μM loperamide; (I) DL-**1**-$SO_3$ with 10 μM troglitazone and 10 μM loperamide; (J) DL-**1**-$SO_3$ with 100 μM BNPP; (K) DD-**1**-$SO_3$; (L) DD-**1**-$SO_3$ with 10 μM troglitazone; (M) DD-**1**-$SO_3$ with 10 μM loperamide; (N) DD-**1**-$SO_3$ with 10 μM troglitazone and 10 μM loperamide; (O) DD-**1**-$SO_3$ with 100 μM BNPP.

**Table S1.** CMC values of the precursors and the hydrogelators.

| | average | st.dev | | average | st.dev |
|---|---|---|---|---|---|
| DL-**1**-$SO_3$ | 916.4 | 8.21 | DL-**1** | 76.1 | 1.22 |
| LD-**1**-$SO_3$ | 929.8 | 6.73 | LD-**1** | 45.7 | 2.43 |
| DD-**1**-$SO_3$ | 939.2 | 5.16 | DD-**1** | 22.1 | 0.89 |

**Table S2.** Compositions and concentrations of the precursors and the hydrogelators.

| | Precursor (μM) | Hydrogelator (μM)[a] |
|---|---|---|
| LD-**1**-$SO_3$ | 0 | 487 |
| DL-**1**-$SO_3$ | 0 | 484 |
| DD-**1**-$SO_3$ | 0 | 491 |

[a]We initially mix the hydrogelator (500 μM) with 4-oxo-4-((2-sulfoethyl)amino)butanoic acid and esterase for 48 h, and the composition of the mixture is analyzed.

**Table S3.** Intracellular concentrations of the precursors and the hydrogelators in HeLa cells.

| LD-**1**-$SO_3$[a] | Precursor (μM) | | Hydrogelator (μM) | |
|---|---|---|---|---|
| | average | st. dev | average | st. dev |
| 1 h | 147.5 | 2.12 | 191.5 | 2.12 |
| 2 h | 161.0 | 1.41 | 258.5 | 4.95 |
| 4 h | 180.5 | 0.71 | 725.5 | 7.78 |
| 8 h | 209.0 | 1.41 | 1242.0 | 5.66 |
| 12 h | 232.0 | 1.41 | 1699.5 | 4.95 |
| DL-**1**-$SO_3$ | | | | |
| 1 h | 119.0 | 1.41 | 188.5 | 3.54 |
| 2 h | 133.5 | 4.95 | 266.5 | 7.78 |
| 4 h | 153.5 | 2.12 | 698.5 | 3.54 |
| 8 h | 174.0 | 2.83 | 1177.5 | 21.92 |
| 12 h | 216.5 | 2.12 | 1644.5 | 9.19 |
| DD-**1**-$SO_3$ | | | | |
| 1 h | 151.5 | 3.54 | 165.5 | 4.95 |
| 2 h | 168.0 | 2.83 | 227.0 | 5.66 |
| 4 h | 186.0 | 5.66 | 694.0 | 11.31 |
| 8 h | 219.5 | 2.12 | 1169.5 | 3.54 |
| 12 h | 239.0 | 1.41 | 1527.5 | 12.02 |

[a]The cell lysates of HeLa cells are collected after 1, 2, 4, 8, 12 h incubation with 100 μM of precursors at 37 ˚C.

**Table S4.** Extracellular concentrations of the precursors and the hydrogelators in culture medium.

| LD-**1**-$SO_3$[a] | Precursor (μM) | | Hydrogelator (μM) | |
|---|---|---|---|---|
| | average | st. dev | average | st. dev |
| 1 h | 88.8 | 1.06 | 5.0 | 0.21 |
| 2 h | 80.3 | 0.42 | 7.8 | 0.07 |
| 4 h | 74.1 | 1.56 | 10.7 | 0.28 |
| 8 h | 70.8 | 0.21 | 14.9 | 0.29 |
| 12 h | 66.4 | 0.57 | 19.4 | 0.85 |
| DL-**1**-$SO_3$ | | | | |
| 1 h | 88.5 | 0.71 | 6.5 | 0.28 |
| 2 h | 80.4 | 0.78 | 8.3 | 0.21 |
| 4 h | 73.9 | 1.63 | 12.4 | 0.49 |
| 8 h | 66.3 | 0.57 | 19.1 | 0.29 |
| 12 h | 61.6 | 0.78 | 25.2 | 0.21 |
| DD-**1**-$SO_3$ | | | | |
| 1 h | 90.5 | 0.71 | 3.8 | 0.28 |
| 2 h | 83.0 | 1.41 | 6.9 | 0.14 |
| 4 h | 78.0 | 2.83 | 8.8 | 0.27 |
| 8 h | 74.6 | 0.57 | 12.6 | 0.57 |

| | | | | |
|---|---|---|---|---|
| 12 h | 71.9 | 0.21 | 15.5 | 0.49 |

[a]The culture media after incubating HeLa cells are collected after 1, 2, 4, 8, 12 h incubation with 100 μM of precursors at 37 ˚C.

**Table S5.** Intracellular concentrations of esterase inhibitors.

| | Intracellular concentration (μM)[a] |
|---|---|
| loperamide | / |
| troglitazone | / |
| BNPP | / |

[a]HeLa cells are incubated with loperamide (10 μM), troglitazone (10 μM) and BNPP (100 μM), respectively for 24 h. Intracellular concentrations are analyzed by using LC-MS.

**Table S6.** Compositions of precursors and hydrogelators after incubating with protease.

| | Precursor (μM)[a] | Hydrogelator (μM)[a] |
|---|---|---|
| LD-**1**-$SO_3$ | 483 | / |
| DL-**1**-$SO_3$ | 479 | / |
| DD-**1**-$SO_3$ | 489 | / |

[a]Precursors (500 μM) are incubated together with protease K (1U/mL) for 24 h.

## 3. Kinetic analysis

### 3.1 Introduction and notation

In this section, we discuss the derivation of the mathematical model used for the kinetic analysis.

The fundamental reaction we want to model is the formation of a supramolecular hydrogel of dipeptide monomers having a terminal alcohol group from the enzyme-catalyzed hydrolysis of an ester precursor. For simpler notation, we use the symbol E for the enzyme, S and P respectively for the molecules of precursors and hydrogelators in solution, and G for the hydrogelators in the assemblies (gel). In the following, we use the terms assemblies and gel interchangeably. We account for the possibility of having precursors trapped in the gel matrix and therefore unable to undergo hydrolysis: in this case we use the symbol Z.

The typical experimental setup consists of a Petri dish where a certain number of tumor cells are put in a cell culture medium with a certain initial concentration of the precursors. The enzyme is present at different concentrations inside the cell and in the culture medium. Hydrolysis and subsequent gel formation can occur both inside and outside the cells, because some of the molecular species in solution cross the cell membrane. In order to distinguish between molecules of a species inside and outside the cells, we use the subscript M for the culture medium and C for the intracellular space. The symbol C without subscripts represents the population of tumor cells in the system.

### 3.1.1 Concentration bracketing

Having different media means that we can define different concentrations for the same species depending on the reference volume. In our model we take into account these different volumes:

- $V_M$ is the volume of the culture medium;
- $V_{cell}$ is the average volume of one single cell;
- $V_C = N_{cell} V_{cell}$ is the total volume of intracellular space, with $N_{cell}$ being the total number of cells;
- $V_{tot} = V_M + V_C$ is the total volume of the system.

We assume that the total system is small enough for the diffusive effects to homogenize the concentration profiles across the system on a very fast time scale. We can therefore work with spatially averaged concentrations- rather than with local concentrations at each point - defined by simply dividing the number of molecules $N_{X^\Phi}$ or the number of moles $n_{X^\Phi}$ of species X in the reference compartment Φ (either M or C) by the appropriate reference volume. We employ the following system of concentration bracketing:

- $\overline{|X^\Phi|} = \frac{N_{X^\Phi}}{V_{tot}}$, molecular concentration in total volume (unit $L^{-1}$);
- $|X^\Phi| = \frac{n_{X^\Phi}}{V_{tot}}$, molar concentration in total volume (unit M = mol $L^{-1}$);
- $[X^\Phi] = \frac{n_{X^\Phi}}{V_\Phi}$, molar concentration in the reference compartment's volume (unit M = mol $L^{-1}$).

A convenient quantity for the present system is the number of cells $N_C$ per unit total volume $V_{tot}$, which can formally be defined as $\overline{|C|}$. This quantity allows us to write a number of useful relations – e.g., $\frac{V_M}{V_{tot}} = 1 - \overline{|C|} V_{cell}$ - to swap from one concentration bracket to another without having to explicitly write the total volume of total cellular space $V_M$, which varies in time with the number of tumor cells.

### 3.2 Derivation of the model

In this section we derive the evolution equations for all the different species in the system. Since we use a continuous, deterministic approach, these equations consist of a set of coupled ordinary differential equations (ODEs). We make the following approximations

- The volume of gel is negligible compared to the volume of the compartment where the gel is formed, so that both $V_M$ and $V_C$ are constant with respect to the gel formation. This is of course true only if the initial concentration of S is not too large, which is always the case in our experiments.
- When a new cell is born or an existing cell dies, the total volume $V_{tot}$ is unaffected. This assumption is justified if the cells are essentially membranes surrounding water solutions. Since the amount of total water solution is conserved, when a cell dies (is born) $V_C$ will decrease (increase) while $V_M$ will increase (decrease) by roughly the same amount.

### 3.2.1 General overview and balance equations

The cellular and molecular species in the system undergo a series of coupled chemical, physical and biological processes sketched in Scheme 3. In general, the molecular species both in the culture medium and in the intracellular space can undergo three types of processes: chemical reactions within the medium where they are contained, physical transport between the two media due to the crossing of the cell membrane, and changes due to cellular birth and death. On the other hand, tumor cells can only undergo two types of biological processes: they can duplicate with constant rate $k_d$, and they can be killed at varying rate $k_k([G^C])$ depending on the intracellular concentration of the gel (i.e., assemblies). The idea behind the latter process is that the chemotherapeutic agent is the gel, which is formed inside the cell and whose killing efficacy increases in a nonlinear fashion with its amount. When the gel kills a tumor cell, we assume that the cell's structure is destroyed so that its original volume and content become part of the culture medium (formally represented by the symbol M in the network at the bottom of Scheme 3).

Based on the above considerations, we can write the general balance equations for the concentrations of all the species with respect to the total volume $V_{tot}$ in the compact form:

$$\frac{d\left|\overline{C}\right|}{dt} = k_d\left|\overline{C}\right| - k_k([G^C])\left|\overline{C}\right| \tag{1}$$

$$\frac{d\left|X^{\Phi}\right|}{dt} = (d_t\left|X^{\Phi}\right|)_{react} + (d_t\left|X^{\Phi}\right|)_{trans} + (d_t\left|X^{\Phi}\right|)_{bio} \tag{2}$$

With X = {S, P, G, Z} and Φ = {M, C}. The three terms on the right-hand side (RHS) of equations (2) respectively account for the reactive processes of hydrolysis plus gel formation, the transport processes across the cell membrane and the variations due to the biological processes of cell birth and death. Since the physically relevant quantities, which enter the reaction and transport terms, are the molar concentrations of the chemical species in the volume of their reference compartment, the first thing that we want to do is to write the left-hand side (LHS) of equations (2) in terms of these variables. For concentrations in the culture medium we have

$$\frac{d\left|X^M\right|}{dt} = \frac{V_M}{V_{tot}}\frac{d[X^M]}{dt} + [X^M]\frac{d}{dt}\left(\frac{V_M}{V_{tot}}\right) = (1-\left|\overline{C}\right|V_{cell})\frac{d[X^M]}{dt} - V_{cell}[X^M]\frac{d\left|\overline{C}\right|}{dt}$$

$$= (1-\left|\overline{C}\right|V_{cell})\frac{d[X^M]}{dt} - (k_d - k_k([G^C]))\left|\overline{C}\right|V_{cell}[X^M] \quad (3)$$

By using analogous arguments, we can also write for the concentrations in the intracellular space

$$\frac{d\left|X^C\right|}{dt} = \left|\overline{C}\right|V_{cell}\frac{d[X^C]}{dt} + (k_d - k_k([G^C]))\left|\overline{C}\right|V_{cell}[X^C] \quad (4)$$

By combining equations (2), (3) and (4) we obtain:

$$\frac{d[X^M]}{dt} = \frac{(d_t\left|X^M\right|)_{react}}{1-\left|\overline{C}\right|V_{cell}} + \frac{(d_t\left|X^M\right|)_{trans} + (d_t\left|X^M\right|)_{bio} + (k_d - k_k([G^C]))\left|\overline{C}\right|V_{cell}[X^M]}{1-\left|\overline{C}\right|V_{cell}} \quad (5)$$

$$\frac{d[X^C]}{dt} = \frac{(d_t\left|X^C\right|)_{react}}{\left|\overline{C}\right|V_{cell}} + \frac{(d_t\left|X^C\right|)_{trans} + (d_t\left|X^C\right|)_{bio}}{\left|\overline{C}\right|V_{cell}} - (k_d - k_k([G^C]))[X^C] \quad (6)$$

The advantage of this formulation with respect to deriving kinetic laws directly for the local concentration $[X^\Phi]$ is that, for the transport and the biological terms, it is more straightforward to derive constitutive relations in terms of concentrations over the total volume. This is however not true for the reactive term, since the natural way to derive the associated kinetic law is through the mass action law, which acts by definition on the local concentrations $[X^\Phi]$ within each compartment. One thing to notice in the above equations is that each term on the RHS takes into account processes that are independent of one another: this means that in the absence of both transport and biological effects, the first term on the RHS of both equations (5) and (6) would be exactly the same. In this case equations (5) and (6) would just describe the chemical kinetics of hydrolysis and gel formation within either the M or the C compartment, which respectively depends only on the local concentrations $[X^M]$ and $[X^C]$. In other words, the first terms on the RHS of equations (5) and (6) must have the form of the chemical kinetics that can be straightforwardly derived from the mass action law in terms of local concentrations, so we can write:

$$\frac{d\left|\overline{C}\right|}{dt} = (k_d - k_k([G^C]))\left|\overline{C}\right| \quad (7)$$

$$\frac{d[X^M]}{dt} = (d_t[X^M])_{react} + \frac{(d_t\left|X^M\right|)_{trans} + (d_t\left|X^M\right|)_{bio} + (k_d - k_k([G^C]))\left|\overline{C}\right|V_{cell}[X^M]}{1-\left|\overline{C}\right|V_{cell}} \quad (8)$$

$$\frac{d[X^C]}{dt} = (d_t[X^C])_{react} + \frac{(d_t|X^C|)_{trans} + (d_t|X^C|)_{bio}}{|\overline{C}|V_{cell}} - (k_d - k_k([G^C]))[X^C] \quad (9)$$

The next steps will be to write appropriate constitutive relations for each of the unknown terms in equations (7)-(9).

### 3.2.2 Chemical reactions

We start by deriving terms $(d_t[X^\phi])_{react}$ associated with the chemical reactions occurring within the M or the C compartment. In general, we assume that there are up to three independent chemical reactions that can occur between the different species in the system: hydrolysis, gelation, and trapping. So we can decompose the reactive term as

$$(d_t[X^\phi])_{react} = (d_t[X^\phi])_{hydr} + (d_t[X^\phi])_{gel} + (d_t[X^\phi])_{trap} \quad (10)$$

#### 3.2.2.1 Hydrolysis

The hydrolysis reaction is the one responsible for breaking the precursor S into an acid (whose concentration we do not keep track of) and the hydrogelator, alcohol P. This reaction is catalyzed by the enzyme E through the formation of the complex ES which then dissociates into P and E. We model this reaction according to the Michaelis-Menten mechanism

$$E + S \underset{k_r}{\overset{k_f}{\rightleftarrows}} ES \xrightarrow{k_{cat}} E + P \quad (11)$$

We experimentally tested the possibility for the above reaction to proceed backwards, i.e., from P to S, by preparing a fresh solution of the hydrogelator P and the enzyme E and measuring the concentrations of both P and S over time. Since no change in the concentration of P was observed, and we did not notice any production of S, we concluded that the conversion of ES into P and E must proceed in irreversibly.

By invoking a quasi-steady state approximation for the concentration of ES, we obtain the classic Michaelis-Menten kinetics

$$v^{\Phi}_{hydr} = [E^{\Phi}]_0 \frac{k_{cat}[S^{\Phi}]}{K_M + [S^{\Phi}]} \ , \quad (12)$$

where the constant $[E^{\Phi}]_0$ is the analytical concentration of enzyme in the compartment Φ and

$$K_M = \frac{k_r + k_{cat}}{k_f} . \quad (13)$$

Equation (12) is valid for both the species in the culture medium and those in the intracellular space. We also assume that the values of the kinetic constants $k_f$, $k_r$ and $k_{cat}$ are the same in both compartments.

### 3.2.2.2 Gelation

The gelation is the reaction by which the hydrogelator monomers P organize into non-covalent polymeric aggregates, which then entangle to form a gel network. We model the gelation as a simple precipitation reaction whose kinetic law – which can be justified on thermodynamic arguments – reads:.

$$v_{gel}^{\Phi} = k_g[P^{\Phi}] - k_s\Gamma([G^{\Phi}]) = k_g([P^{\Phi}] - K_{gs}^{-1}\Gamma([G^{\Phi}])), \tag{14}$$

where $k_g$, $k_s$ and $K_{gs}$ are constants and $\Gamma([G^{\Phi}])$ is the step function

$$\Gamma(x) = \begin{cases} 0 & if \quad x \le 0 \\ 1 & if \quad x > 0 \end{cases}. \tag{15}$$

We added the step function $\Gamma([G^{\Phi}])$ to account for the fact that the chemical potential of G is defined only if there are molecules of G (or in other words, if $[G^{\Phi}] > 0$) in the Φ compartment; if no G molecules are present, the reaction proceeds irreversibly from P to G.

*Effect of the precursor on the gelation process***.** So far we have assumed that the only species responsible for the formation of the gel is the hydrogelator P. Experiments, however, show that the precursor S also has the ability to form hydrogels at large enough concentrations. Since both species can form hydrogels, we cannot *a priori* exclude the possibility that the presence of the precursor may affect the hydrogelation properties of the hydrogelator. In order to check if this is the case, we have experimentally measured the critical concentration for the gel formation - to which we refer as CMC, since the experimental technique we used is the same as the one to determine the critical micelle concentration in surfactant solutions - for solutions of hydrogelator and precursor with varying percentage of precursor: 0% (only the hydrogelator), 25%, 50%, 75% and 100% (only the precursor). The trend for the DL-**1**-$SO_3$, LD-**1**-$SO_3$ and DD-**1**-$SO_3$ stereoisomers (see Figure S9) shows that the larger the precursor percentage the higher the CMC. This can be due either to an interaction between the precursor and the hydrogelator or simply because of dilution effects of the hydrogelator content as its percentage decreases, which would therefore require higher total concentrations to reach the same CMC value of the hydrogelator-only solution. To test the validity of this second hypothesis, we assumed that the hydrogelator concentration required to form the gel would be independent on the concentration of the precursor, so we projected the value $CMC_0$ of the CMC for the hydrogelator-only solution for the different values of precursor percentage %s assuming that this would only entail a simple dilution effect according to the expression

$$CMC_{model} = \frac{CMC_0}{1 - 0.01\%_S} \quad (16)$$

Figure S9 shows a direct comparison between the experimentally measured CMC values and the theoretical values $CMC_{model}$. As we can see, the hypothesis behind equation (16) closely matches the experimental data for a very large range of compositions, at least up to 75% composition in precursor. The deviations between the model and the experiments are larger for the DL-**1**-$SO_3$, than the LD-**1**-$SO_3$ than the DD-**1**-$SO_3$ stereoisomers, but in all three cases they may be noticeable only for highly concentrated solutions. Since in our experiments we work with solutions up to a maximum initial precursor concentration of 500 μM (for which no gelation is observed), we can therefore neglect both the gelation of S and any possible co-precipitation effects between S and P. We will therefore continue to assume - as we did so far - that the gel formation is exclusively driven by the precipitation of the hydrogelators. Under these conditions we have

$$K_{gs}^{-1} = CMC_0 \quad (17)$$

### 3.2.2.3 Trapping

The third chemical reaction that we take into account is the trapping of precursor molecules within the gel network of the hydrogelator during gelation. We needed to include such a process in our model in order to rationalize the trends observed in experimental data for the hydrolysis of the DL-**1**-$SO_3$, LD-**1**-$SO_3$ and DD-**1**-$SO_3$ ester in the absence of cells.

*Justification.* When the enzyme E is added to a solution of the precursor S, we observe that the concentration of S decreases over time due to the hydrolysis reaction (11) and the subsequent gel formation. Since the second step of the Michaelis-Menten scheme (11) is irreversible, we should see the concentration of S drop to zero asymptotically in time. However this is not what happens when the reaction is run in an aqueous solution in the absence of cells (see Figure S12): what we observe instead is that for different initial concentrations, the measured concentration of S approaches different nonzero plateau. This trend, which is qualitatively true for all three stereoisomers, can be explained by assuming that some molecules of S are "trapped" within the gel network formed by the P molecules and are therefore unable to participate in the hydrolysis reaction (11): since what we measure experimentally is the total concentration of S molecules - whether trapped in the gel or free in the solution - this pool of trapped and nonreactive S molecules will keep the total measured concentration of S larger than zero even after all the S molecules in the solution have irreversibly been hydrolyzed.

This trapping hypothesis is justified on the basis that in an aqueous solution of mostly S and a catalytic concentration of E, the newly formed gel clusters will have a high probability to encounter an S molecule and therefore include it in some of the vacancies of the gel network. The same process becomes however quite unlikely when the gel is formed in the highly crowded

and structured intracellular space, especially given the fact that the S molecules are gradually transported inside the cell from the culture medium and they never get the chance to accumulate too much before being converted to P and then to G. We therefore assume no trapping mechanism for the intracellular gel formation.

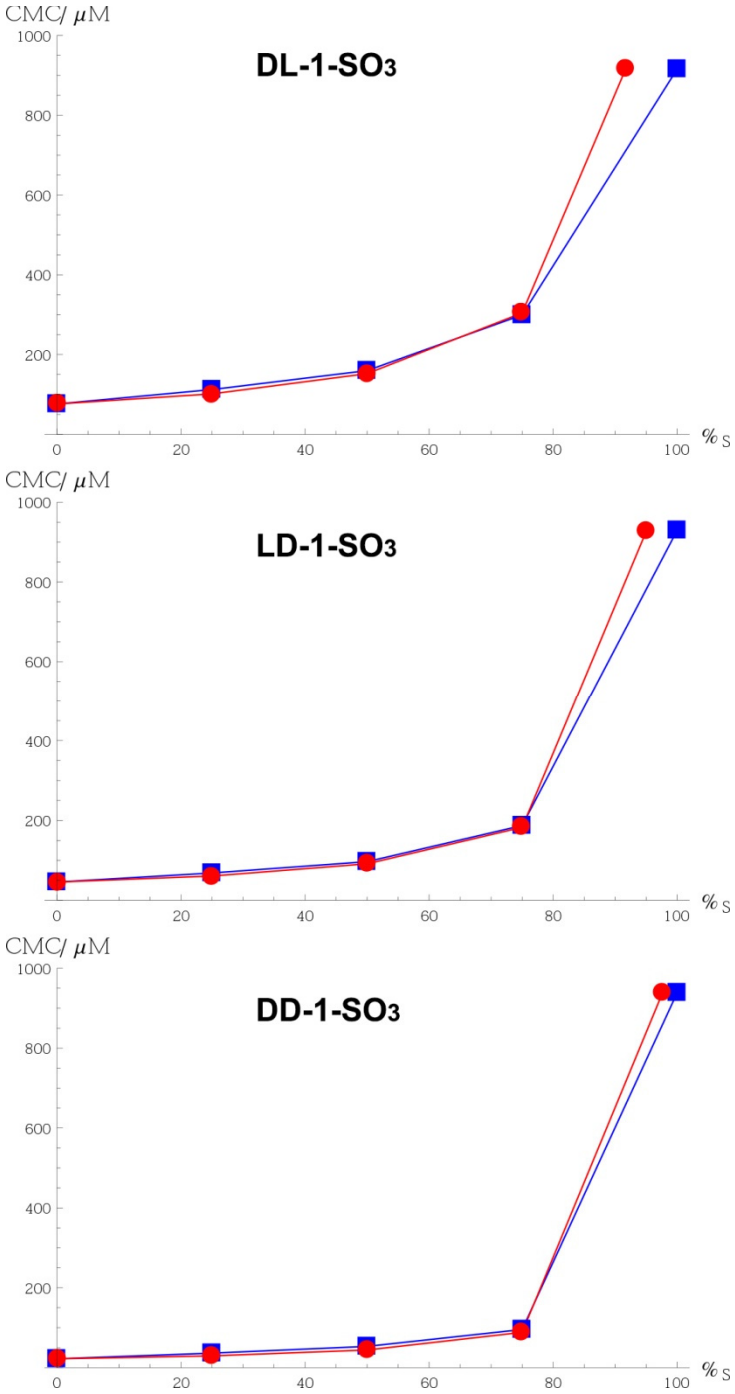

**Figure S9.** Comparison between the experimentally measured CMC values (blue squares) and $CMC_{model}$ (red disks) for different percentages %s of precursor, for the three stereoisomers DL-**1**-$SO_3$ (top), LD-**1**-$SO_3$ (middle), DD-**1**-$SO_3$ (bottom). The CMC is expressed in μM units.

*Modeling.* The trapping reaction occurs when some molecules of S get surrounded and trapped by polymers of P molecules as soon as the latter assemble into the gel G. A simple but effective way to model this situation is to idealize the trapping as an irreversible and immediate "adsorption" of S molecules on the newly formed layers of G according to the reaction scheme

$$S + *_G \xrightarrow{k_{trap}} Z, \tag{18}$$

Where $*_G$ represents an empty spot in the gel network available to S, and Z is the symbol that we use to identify the trapped S molecules. The associated reaction rate reads

$$v_{trap}^{\Phi} = k_{trap}[S^{\Phi}][*_G^{\Phi}] \tag{19}$$

The concentration of free empty sites $[*_G^{\Phi}]$ directly (we assume linearly) depends on the concentration of G and is reduced by the concentration of Z:

$$[*_G^{\Phi}] = \zeta[G^{\Phi}] - [Z^{\Phi}] \tag{20}$$

Where ζ is a gel-specific constant representing the average number of empty sites in the gel structure per molecule of G available to the inclusion of one molecule of S. The velocity of the trapping reaction therefore reads

$$v_{trap}^{\Phi} = k_{trap}[S^{\Phi}](\zeta[G^{\Phi}] - [Z^{\Phi}]) \tag{21}$$

It is important to notice that in order for the above model to be representative of the physical picture we outlined above, we must at some point let $k_{trap} \to \infty$. This condition will be used afterwards in the form of a quasi-steady-state approximation for the concentration of Z when deriving the final form of the evolution equations in subsection 3.2.5.1.

### 3.2.3 Transmembrane transport

Now we want to derive suitable expressions for the rates of transport $v_{in}^{X}$ and $v_{out}^{X}$ of a certain species X from the culture medium to the intracellular space and from the intracellular space to the culture medium. In order to model the transport of molecules across the cell membrane, we start from microscopic arguments and then derive appropriate average mean-field equations.

We start by breaking down the transport process in the sum of two independent processes: transport of molecules from the culture medium M to the intracellular space C and transport from C to M. We assume that both these transport processes are passive and driven only by simple

random motion of the molecules, and we also approximate the cell membrane to a simple semipermeable membrane.

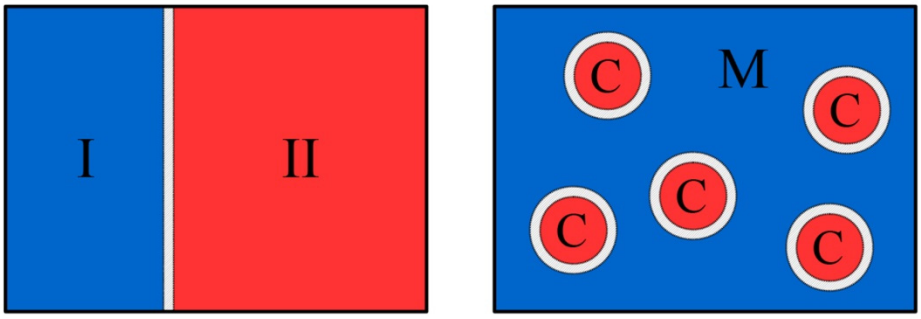


**Figure S10.** Schematic representation of the two ideal systems used to derive the transport term. On the left, a system composed by two compartments (I and II) separated by a semipermeable membrane. On the right, a system composed by a number of vesicles (idealizing the cells, whose total inside space we refer as C) surrounded by an external medium (in our case being the culture medium, labeled as M).

In order to gain insight on these two processes, we first notice that if we have two compartments I and II (see left picture in Figure S10) separated by a membrane, which is permeable to the molecules of a certain species X, the transport from - say - compartment I to compartment II will be possible only if there is a molecule in compartment I that will hit the membrane with the right energy and orientation and if there is enough room for the molecule in compartment II after it has crossed the membrane. From these considerations, we can estimate that

$$v^{X}_{I\to II} \propto \frac{A_{surf}}{V_{tot}}[X^{I}][*^{II}_{X}] \tag{22}$$

$$v^{X}_{II\to I} \propto \frac{A_{surf}}{V_{tot}}[X^{II}][*^{I}_{X}] \ . \tag{23}$$

Notice that the reference bulk concentrations of $X^{I}$, $X^{II}$, $*^{I}_{X}$ and $*^{II}_{X}$ must be relative to the volume of the respective compartments, and not to the total volume.

If we now consider the situation (see right picture in Figure S10) where one of the two compartments - let's call it C - is a collection of small volumes entirely surrounded by the semipermeable membrane and immersed in the volume of the other compartment - which we now call M - the above physical arguments remain exactly the same with $v^{X}_{M\to C}$ and $v^{X}_{I\to II}$ being exactly $v^{X}_{in}$ and $v^{X}_{out}$. If we call $A_{cell}$ the average area of one single cell, we can express the total area of cell membrane per total volume as

$$\frac{A_{surf}}{V_{tot}} = A_{cell}\frac{N_C}{V_{tot}} = A_{cell}\left|\overline{C}\right|, \tag{24}$$

So that the two transport rates read

$$v_{in}^{X} \propto A_{cell}\left|\overline{C}\right|[X^M][*_X^C] \tag{25}$$

$$v_{out}^{X} \propto A_{cell}\left|\overline{C}\right|[X^C][*_X^M]\ . \tag{26}$$

If we assume that the concentrations of empty sites $[*_X^M]$ and $[*_X^C]$ both in the medium and in the intracellular space is large enough to be considered as a constant, we can express the rates for the inside and outside transport processes as

$$v_{in}^{X} = k_{in}^{X} V_{cell}\left|\overline{C}\right|[X^M] \tag{27}$$

$$v_{out}^{X} = k_{out}^{X} V_{cell}\left|\overline{C}\right|[X^C], \tag{28}$$

Where for convenience reasons we have explicitly multiplied by the cell volume and included the area dependence inside the two proportionality constants $k_{in}^{X}$ and $k_{out}^{X}$, which are entirely system specific.

In our model, we assume that only S can cross the membrane. The species G and Z cannot cross the membrane because they are part of a gel network which is too large. In principle P could also cross the membrane, but for the sake of simplicity we will neglect its transport. The reason is that the concentration of P quickly equilibrates to its constant CMC value because of the gelation process both inside and outside the cells, thus creating a zero gradient across the membrane and instantly reverting any change due to transport. This makes the precise fitting of $k_{in}^{P}$ and $k_{out}^{P}$ from our available data particularly difficult and unreliable. We therefore prefer to incorporate all the possible kinetic effect due to the transport of molecules that would eventually produce G in $k_{in}^{S}$ and $k_{out}^{S}$, which then play the role of defining an overall effective diffusion of molecules between the inside and the outside of the cells.

### 3.2.4 Cellular proliferation and death

In this subsection, we derive appropriate expressions for the terms $(d_t\left|X^{\Phi}\right|)_{bio}$ which represent the changes that occur to the total concentrations $|X^{\Phi}|$ of the molecular species when cells are born and killed. Since the two biological processes that occur to the tumor cells are the birth of new cells and the death of existing cells induced by the intracellular gel, we can divide the above term as the sum of two quantities:

$$(d_t \left| X^{\Phi} \right|)_{bio} = (d_t \left| X^{\Phi} \right|)_{birth} + (d_t \left| X^{\Phi} \right|)_{death} . \quad (29)$$

### 3.2.4.1 Cell proliferation

A preliminary consideration is that we do not take into account any natural death process for the tumor cells: one of the problems of tumor cells is that they do not naturally die, but they just keep on doubling their population with rate $k_d \left| \overline{C} \right|$. We refer to this process as the cell proliferation or doubling.

Recall that a fundamental assumption we make in this model is that the total volume $V_{tot} = V_M + V_C$ is constant. This means that when a new cell is born, thus increasing $V_C$, it occupies some volume that was part of $V_M$. But when this happens the number of molecules of any given species X that is present in either the M or C compartments do not change: when a cell duplicates, its content is now shared between the two new cells, which keeps the number of molecules inside the C compartment (given by the collection of all the cells) constant. As a result the concentrations $[X^M]$ of the species in the culture medium increase, while the concentrations $[X^C]$ of the species inside the intracellular space get more diluted. However, since both the number of molecules inside the two compartments and the total volume stay constant, the concentrations $|X^M|$ and $|X^C|$ hardly change because of the cell birth process. Since the term $(d_t \left| X^{\Phi} \right|)_{birth}$ accounts for the changes of these latter concentrations, we can safely say that

$$(d_t \left| X^{\Phi} \right|)_{birth} = 0 \ . \quad (30)$$

### 3.2.4.2 Cell death

Cells are killed with rate $k_k([G^C])\left| \overline{C} \right|$ which depends on the average concentration of G inside the cells. Once again, the advantage of working with concentrations over total volume $|X^M|$ is that we do not need to care about the changes in the volume of M or C and just focus on which compartment the molecules of X are. When a cell dies, we assume that its structure is eventually lost and therefore its content and volume become part of the extracellular medium. If every cell contains a number of moles $n_X^{cell}$ of X, when a number $k_k([G^C])\left| \overline{C} \right|$ of cells die in the unit time, they will release a number of moles $k_k([G^C])\left| \overline{C} \right| n_X^{cell}$ of X in the culture medium. We can therefore write

$$v_{death}^X = k_k([G^C])\left| \overline{C} \right| n_X^{cell} = k_k([G^C]) V_{cell} \left| \overline{C} \right| \frac{n_X^{cell}}{V_{cell}} \quad (31)$$

In our mean-field approach this means

$$\frac{n_X^{cell}}{V_{cell}} = \frac{n_X^C}{V_C} = [X^C] \tag{32}$$

And hence

$$v_{death}^X = k_k([G^C])V_{cell}\overline{|C|}[X^C] \ . \tag{33}$$

### 3.2.4.3 Killing rate constant

Finally we want to derive an explicit expression for the killing rate constant $k_k([G^C])$. Unfortunately we do not have too much information about the microscopic interaction between the gel and the cells and how the killing process precisely occurs. We know that in general cells die more quickly when the concentration of gel inside the cells is large. So we know that $k_k([G^C])$ must be a direct function of $[G^C]$ and that $k_k([G^C]) = 0$ for $[G^C] = 0$. The simplest function that comes to mind with these properties is of course a linear function $k_k([G^C]) = \text{cst}\ [G^C]$, but when we tried to fit the cytotoxicity data with this function we did not obtain a very good match between the model and the experimental data.

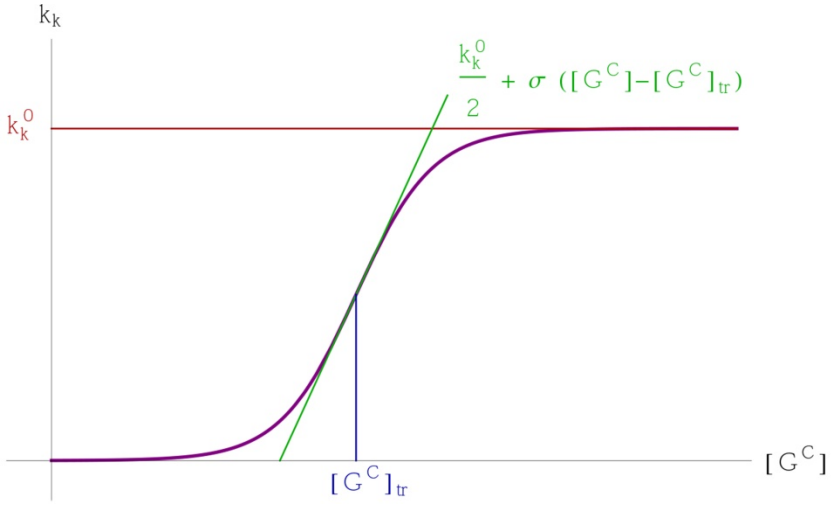


**Figure S11.** Plot of the general shape of the killing rate constant $k_k([G^C])$ as a function of $[G^C]$. The function defined by equation (34) is plotted in purple. The red and blue straight lines respectively show the position of $k_k^0$ and $[G^C]_{tr}$, while the green straight line has the same slope as $k_k([G^C])$at the inflexion point.

We therefore decided to use a nonlinear "S-shaped" functional which starts from zero, slowly increases until it comes in the proximity of a threshold value $[G^C]_{tr}$ at which point the slope increases to a value σ, and then asymptotically approaches a plateau value $k_k^0$ (see Figure S11). Among all the possible sigmoidal functions with these properties, we chose to use the hyperbolic tangent functional

$$k_k([G^C]) = \frac{k_k^0}{2}(1+\tanh(2\sigma([G^C]-[G^C]_{tr}))). \tag{34}$$

### 3.2.5 Final equations

Now that we have constitutive relations for all the processes occurring in our system, we can finally combine them to obtain the final form of the evolution laws for the concentration variables. Let's start by re-writing equations (8)-(9) in the more explicit form

$$\frac{d[X^M]}{dt} = (d_t[X^M]_{hydr} + (d_t[X^M])_{gel} + d_t[X^M])_{trap} + \frac{(d_t|X^M|)_{trans}}{1-|\overline{C}|V_{cell}}$$

$$+\frac{|\overline{C}|V_{cell}}{1-|\overline{C}|V_{cell}}(\frac{(d_t|X^M|)_{death}}{|\overline{C}|V_{cell}} + (k_d - k_k([G^C]))[X^M] \tag{35}$$

$$\frac{d[X^C]}{dt} = (d_t[X^C])_{hydr} + (d_t[X^C])_{gel} + \frac{(d_t|X^C|)_{trans}}{|\overline{C}|V_{cell}} + \frac{(d_t|X^C|)_{death}}{|\overline{C}|V_{cell}} - (k_d - k_k([G^C]))[X^C]\,. \tag{36}$$

**Table S7.** Summary of the kinetic terms in the evolution laws for each of the molecular variables in our model.

| $X^\Phi$ | $\left(d_t[X^\Phi]\right)_{hydr}$ | $\left(d_t[X^\Phi]\right)_{gel}$ | $\left(d_t[X^\Phi]\right)_{trap}$ | $\left(d_t\|X^\Phi\|\right)_{trans}$ | $\left(d_t\|X^\Phi\|\right)_{death}$ |
|---|---|---|---|---|---|
| $S^M$ | $-v^M_{hydr}$ | $0$ | $-v^M_{trap}$ | $-v^S_{in} + v^S_{out}$ | $+v^S_{death}$ |
| $P^M$ | $+v^M_{hydr}$ | $-v^M_{gel}$ | $0$ | $0$ | $+v^P_{death}$ |
| $G^M$ | $0$ | $+v^M_{gel}$ | $0$ | $0$ | $0$ |
| $Z^M$ | $0$ | $0$ | $+v^M_{trap}$ | $0$ | $0$ |
| $S^C$ | $-v^C_{hydr}$ | $0$ | $0$ | $+v^S_{in} - v^S_{out}$ | $-v^S_{death}$ |
| $P^C$ | $+v^C_{hydr}$ | $-v^C_{gel}$ | $0$ | $0$ | $-v^P_{death}$ |
| $G^C$ | $0$ | $+v^C_{gel}$ | $0$ | $0$ | $-v^G_{death}$ |

The five contributions in the above equations for each variable can be found by multiplying the rate of the respective process by the net stoichiometric coefficient of the species in that process. Table S7 offers a schematic summary of the different terms for the seven molar concentration variables in our system. The different terms in Table S7 are defined by equations (12), (14), (21), (27), (28) and (33). The system is therefore fully described by the following eight evolution equations:

$$\frac{d\overline{|C|}}{dt} = (k_d - k_k([G^C]))\overline{|C|} \tag{37}$$

$$\frac{d[S^M]}{dt} = -\frac{[E^M]_0 k_{cat}[S^M]}{K_M + [S^M]} - k_{trap}[S^M](\zeta[G^M] - [Z^M])$$

$$-\frac{\overline{|C|}V_{cell}}{1-\overline{|C|}V_{cell}}(k_{in}^S[S^M] - k_{out}^S[S^C]) + \frac{\overline{|C|}V_{cell}}{1-\overline{|C|}V_{cell}}(k_d[S^M] - k_k([G^C])([S^M] - [S^C])) \tag{38}$$

$$\frac{d[P^M]}{dt} = +\frac{[E^M]_0 k_{cat}[S^M]}{K_M + [S^M]} - k_g([P^M] - K_{gs}^{-1}\Gamma([G^M]))$$

$$+\frac{\overline{|C|}V_{cell}}{1-\overline{|C|}V_{cell}}(k_d[P^M] - k_k([G^C])([P^M] - [P^C])) \tag{39}$$

$$\frac{d[G^M]}{dt} = +k_g([P^M] - K_{gs}^{-1}\Gamma([G^M])) + \frac{\overline{|C|}V_{cell}}{1-\overline{|C|}V_{cell}}(k_d - k_k([G^C]))[G^M] \tag{40}$$

$$\frac{d[Z^M]}{dt} = +k_{trap}[S^M](\zeta[G^M] - [Z^M]) + \frac{\overline{|C|}V_{cell}}{1-\overline{|C|}V_{cell}}(k_d - k_k([G^C]))[Z^M] \tag{41}$$

$$\frac{d[S^C]}{dt} = -\frac{[E^C]_0 k_{cat}[S^C]}{K_M + [S^C]} + k_{in}^S[S^M] - k_{out}^S[S^C] - k_d[S^C] \tag{42}$$

$$\frac{d[P^C]}{dt} = +\frac{[E^C]_0 k_{cat}[S^C]}{K_M + [S^C]} - k_g([P^C] - K_{gs}^{-1}\Gamma([G^C])) - k_d[P^C] \tag{43}$$

$$\frac{d[G^C]}{dt} = +k_g([P^C] - K_{gs}^{-1}\Gamma([G^C])) - k_d[G^C] \tag{44}$$

*Gel release because of cell death.* While most terms in Table 1 can be straightforwardly derived based on what we have said so far, we feel that some comments are due in regard to the death term for $G^M$. Equation (40) is derived by assuming

$$(d_t\left|G^M\right|)_{death} = 0 \tag{45}$$

Instead of $(d_t\left|G^M\right|)_{death} = +v_{death}^G$, as it would be expected by simply looking at the general form of equation (35). The translation of (45) in physical terms is that when the cells die the amount of gel inside them does not add up to the pool of gel already present in the culture medium. The

reason of this choice is that the two types of gels have very different composition and structure and it would therefore not be a wise choice to simply assume that they can both be described as $G^M$, even if they are both present in the medium.

### 3.2.5.1 Fast trapping

In section 3.2.2.3, we stated that in order for our modelling of the trapping mechanism to be effective, we need to let $k_{trap} \to \infty$. This means that the first term in (41) reaches its equilibrium value in a much faster time scale than the second term. As we hinted back in section 3.2.2.3, this implies that the value of $[Z^M]$ can be considered always in a quasi-steady state given by the solution of

$$k_{trap}[S^M](\zeta[G^M]-[Z^M]) = 0, \tag{46}$$

Or in other words

$$[Z^M] = \zeta[G^M]. \tag{47}$$

It is important to notice that this condition makes sense only if $[S^M] \neq 0$, and it states that as long as we have S in the solution, we will form a gel with a constant composition in Z.

Thanks to the above condition, we can rearrange equation (41) as

$$\begin{aligned} k_{trap}[S^M](\zeta[G^M]-[Z^M]) &= \frac{d[Z^M]}{dt} - \frac{\overline{|C|}V_{cell}}{1-\overline{|C|}V_{cell}}(k_d - k_k([G^C]))[Z^M] \\ &= \zeta\left(\frac{d[G^M]}{dt} - \frac{\overline{|C|}V_{cell}}{1-\overline{|C|}V_{cell}}(k_d - k_k([G^C]))[G^M]\right) \\ &= \zeta k_g([P^M] - K_{gs}^{-1}\Gamma([G^M])), \end{aligned} \tag{48}$$

Which allows to re-write the balance equation (54) for S as

$$\begin{aligned} \frac{d[S^M]}{dt} = &-\frac{[E^M]_0 k_{cat}[S^M]}{K_M + [S^M]} - \zeta k_g([P^M] - K_{gs}^{-1}\Gamma([G^M])) - \frac{\overline{|C|}V_{cell}}{1-\overline{|C|}V_{cell}}(k_{in}^S[S^M] - k_{out}^S[S^C]) \\ &+ \frac{\overline{|C|}V_{cell}}{1-\overline{|C|}V_{cell}}(k_d[S^M] - k_k([G^C])([S^M]-[S^C])). \end{aligned} \tag{49}$$

Equation (49) together with equations (37), (39), (40), (42), (43) and (44) form now a system of seven closed equation in seven variables which can be numerically integrated to fit the experimental data.

### 3.2.5.2 Nondimensionalization

In order to facilitate the fittings and have a better comparison between the different datasets, it is convenient to partially nondimensionalize the evolution laws by properly scaling some of the variables and parameters.

Since all the experiments start with an initial number $\left|\overline{C}\right|_0$ of cells per total volume, an initial concentration $[S^M]_0$ of $S^M$ and zero concentrations of all the other species (except the enzyme), it is reasonable to scale all the molecular concentrations (except the enzyme's one) by $[S^M]_0$ and $\left|\overline{C}\right|$ by $\left|\overline{C}\right|_0$:

$$s^M = \frac{[S^M]}{[S^M]_0}, \qquad p^M = \frac{[P^M]}{[S^M]_0}, \qquad g^M = \frac{[G^M]}{[S^M]_0}, \qquad z^M = \frac{[Z^M]}{[S^M]_0} \tag{50}$$

$$s^C = \frac{[S^C]}{[S^M]_0}, \qquad p^C = \frac{[P^C]}{[S^M]_0}, \qquad g^C = \frac{[G^C]}{[S^M]_0}, \qquad c = \frac{\left|\overline{C}\right|}{\left|C\right|_0}. \tag{51}$$

As for the enzyme, since we adopt a Michaelis-Menten kinetics we are only interested in its analytical concentration $[E]_0$. This value is different inside and outside the cells, therefore we need to somehow keep track of both $[E^M]_0$ and $[E^C]_0$. The situation is complicated by the fact that the enzyme concentration $[E^h]_0$ relative to the dataset used to fit the kinetic constants of the hydrolysis/gelation/trapping reactions - see section 3.2 - is different from both $[E^M]_0$ and $[E^C]_0$. Instead of trying to fit the actual values of $[E^h]_0$, $[E^M]_0$ and $[E^C]_0$ we prefer to define a scaled version of $k_{cat}$ by $[E^h]_0$ and use the ratio between the different enzyme concentrations as fitting parameters:

$$\%k_{cat} = [E^h]_0 k_{cat}, \qquad \delta^M = \frac{[E^M]_0}{[E^h]_0}, \qquad \delta^C = \frac{[E^C]_0}{[E^h]_0}. \tag{52}$$

For the sake of a simpler notation we also set

$$C_0 = \left|\overline{C}\right| V_{cell}, \qquad S_0 = [S^M]_0, \qquad k_{in}^S = k_{in}, \qquad k_{out}^S = k_{out}. \tag{53}$$

Thanks to these definitions we can re-write the governing equations of our system as

$$\frac{dc}{dt} = (k_d - k_k(S_0 g^C))c \tag{54}$$

$$\frac{ds^M}{dt} = -\frac{\delta^M \%k_{cat} s^M}{K_M + S_0 s^M} - \zeta k_g (p^M - K_{gs}^{-1}\Gamma(g^M)) - \frac{C_0 c}{1 - C_0 c}(k_{in} s^M - k_{out} s^C)$$

$$+\frac{C_0 c}{1-C_0 c}(k_d s^M - k_k(S_0 g^C)(s^M - s^C)) \tag{55}$$

$$\frac{dp^M}{dt} = +\frac{\delta^M \%k_{cat} s^M}{K_M + S_0 s^M} - k_g(p^M - K_{gs}^{-1}\Gamma(g^M)) + \frac{C_0 c}{1-C_0 c}(k_d p^M - k_k(S_0 g^C)(p^M - p^C)) \tag{56}$$

$$\frac{dg^M}{dt} = +k_g(p^M - K_{gs}^{-1}\Gamma(g^M)) + \frac{C_0 c}{1-C_0 c}(k_d - k_k(S_0 g^C))g^M \tag{57}$$

$$\frac{ds^C}{dt} = -\frac{\delta^C \%k_{cat} s^C}{K_M + S_0 s^C} + k_{in} s^M - k_{out} s^C - k_d s^C \tag{58}$$

$$\frac{dp^C}{dt} = +\frac{\delta^C \%k_{cat} s^C}{K_M + S_0 s^C} - k_g(p^C - K_{gs}^{-1}\Gamma(g^C)) - k_d p^C \tag{59}$$

$$\frac{dg^C}{dt} = +k_g(p^C - K_{gs}^{-1}\Gamma(g^C)) - k_d g^C \tag{60}$$

The above set of ODEs - or suitable subsets of it - can be numerically integrated with initial conditions

$$c(0) = s^M(0) = 1 \qquad and \qquad p^M(0) = g^M(0) = s^C(0) = p^C(0) = g^C(0) = 0 \tag{61}$$

To fit the values of the control parameters on the experimental data.

### 3.3 Data fitting

In this section, we use the general model (54)-(60) to estimate the values of the control parameters from experimental data. Our aim is to compare the values for the DL-**1**-$SO_3$, LD-**1**-$SO_3$, and DD-**1**-$SO_3$ stereoisomers, and to understand the reason behind their different cytotoxicity. The model contains 15 parameters which we conveniently divide into 4 groups:

- *Group 0:* $S_0$, $C_0$, $k_d$, $k_g$, $K_{gs}$. Parameters that we can directly measure or estimate from the literature.
- *Group 1:* $\%k_{cat}$, $K_M$, $\zeta$. Parameters related to the chemical reactions occurring within each compartment.
- *Group 2:* $\delta^M$, $\delta^C$, $k_{in}$, $k_{out}$. Parameters related to the transport between M and C and to the different enzymatic concentrations in the two compartments.
- *Group 3:* $k_k^0$, $\sigma$, $[G^C]_{tr}$. Parameters characterizing the cytotoxicity of the intracellular gels.

While the parameters in Group 0 do not require to be fitted, we use a numerical fitting procedure to obtain the values of the other parameters. Our approach is to fit Group 1, Group 2 and Group 3 in this order, on datasets coming from ad-hoc experiments**.**

All the fittings are performed by using the FindFit function of Mathematica, with the NMinimize method option, starting from default initial conditions and with no constraints on the parameters range. The ODE solver used in the fitting algorithm is the ParametricNDSolveValue function of Mathematica with default options. In order to facilitate the fittings, we introduce each parameter $\Theta$ as a power of 10, so that we effectively fit $\log_{10}\Theta$.

### 3.3.1 Known parameters (Group 0)

*Initial concentrations of precursor.* We perform experiments with different initial concentrations $S_0$ of precursor, ranging from 20 to 500 μM. The exact values of $S_0$ will be given for each dataset.

*Number of cells, cell volume and volume of culture medium.* We can calculate the value of the parameter $C_0 = \dfrac{N_{cell}V_{cell}}{V_M + N_{cell}V_{cell}}$ starting from the known values of the number of cells $N_{cell}$, the cell volume $V_{cell}$ and the volume of culture medium $V_M$. The volume of aqueous precursor solution used in all experiments is $V_M = 10$ mL. The number of cells used in the experiments relative to groups 2 and 3 is $N_{cell} = 2\times10^6$. The average cell volume for the types of tumor cells we use is $V_{cell} = 5000\ \mu m^3$. As a result we can estimate $C_0 = 10^{-3}$.

*Cell doubling rate constant.* The reported doubling time for the type of cells we use is $t_d = 1$ day. We can estimate the doubling rate constant as $k_d = \dfrac{\ln 2}{t_d} = 4.81\times10^{-4}\ \text{min}^{-1}$.

*Gelation rate constant.* One of our assumptions is that the gelation of P into G is a very fast process. One way to use this assumption could be to derive a quasi-steady state approximation for P or a pre-equilibrium approximation for the gelation process itself. However, given the discontinuous nature of the gelation kinetic law, such approaches would either not give a satisfactory representation of the early stages of the kinetics, or produce a much more complicated set of evolution laws. For this reason, we prefer to keep the expression of the gelation kinetics as it is and implement its fast time scale in a purely numerical way, by assigning a wisely chosen arbitrary large value to $k_g$. A value of $10^5\ \text{min}^{-1}$ ensures that the time scale of the gelation process (when it occurs) is much faster than any other time scale in the model. Larger values of $k_g$ do not appreciably change the final global dynamics, while making the fitting code computationally more demanding. Hence we set $k_g = 10^5\ \text{min}^{-1}$.

*Gelation equilibrium constant.* The equilibrium constant $K_{gs}$ for the gelation process of each of the stereoisomers can be directly calculated from the values of $CMC_0$ measured in the experiments plotted in Figure 2, by using equation (17). The values of $CMC_0$ and $K_{gs}$ for the three stereoisomers are:

$$CMC_0^{DL} = 76.1\mu M, \qquad K_{gs}^{DL} = 1.31\times10^{-2}\,\mu M^{-1}\ , \tag{62}$$

$$CMC_0^{LD} = 45.7\mu M, \qquad K_{gs}^{LD} = 2.19\times10^{-2}\,\mu M^{-1}, \tag{63}$$

$$CMC_0^{DD} = 22.1\mu M, \qquad K_{gs}^{DD} = 4.52\times10^{-2}\,\mu M^{-1}. \tag{64}$$

### 3.3.2 Chemical reactions (Group 1)

In order to fit the parameters of group 1, we isolated the kinetics of hydrolysis and gel formation by performing experiments in absence of cells. For each stereoisomer, we measured the variation of the concentration of precursor in time starting from three initial precursor concentrations: 100, 200, and 500 μM. The analytical concentration of enzyme is the same for all the experiments.

Since the physically measurable quantities are the total concentrations of precursor and hydrogelator - regardless if in solution or in the gel form - we define the two additional variables

$$w = s + z \qquad and \qquad y = p + g \tag{65}$$

And derive suitable evolution laws for them. The experiments are then fully described by the following subset of our model:

$$\frac{dw}{dt} = -\frac{k_{cat}^{0}\,s}{K_M + S_0 s} \tag{66}$$

$$\frac{dy}{dt} = +\frac{k_{cat}^{0}\,s}{K_M + S_0 s} \tag{67}$$

$$\frac{ds}{dt} = -\frac{k_{cat}^{0}\,s}{K_M + S_0 s} - \zeta k_g\left(p - K_{gs}^{-1}\Gamma(g)\right) \tag{68}$$

$$\frac{dp}{dt} = +\frac{k_{cat}^{0}\,s}{K_M + S_0 s} - k_g\left(p - K_{gs}^{-1}\Gamma(g)\right) \tag{69}$$

$$\frac{dg}{dt} = +k_g\left(p - K_{gs}^{-1}\Gamma(g)\right). \tag{70}$$

In order to find the value of $k_{cat}^{0}$, $K_M$ and ζ we numerically integrate equations (66)-(70) and fit the simulated time series of w - i.e. the total concentration of precursor - on the experimentally measured values after 1, 2, 4, 6, 8, 12, 24 and 36 hours.

The fittings have been performed in a multivariate fashion and by considering the three stereoisomers separately: for each stereoisomer we fitted the values of $k_{cat}^{0}$, $K_M$ and ζ on the three time series relative to different $S_0$ at the same time (effectively considering $S_0$ as an additional

independent variable just like the time). The outcome of the fitting is shown in Figure S12. The fitted values of the parameters are reported in the summary Table 1.

One thing to notice in Figure S12 is that, although our model qualitatively reproduces the trend of all the three stereoisomers, the quantitative agreement is better for DD-**1**-$SO_3$ than for LD-**1**-$SO_3$ than for DL-**1**-$SO_3$. This echoes the trend observed in Figure S9 for the discrepancies between the values of CMC calculated with equation (16) and the experimentally measured values. Remember that equation (16) is a direct consequence of our assumption that the gelation of the hydrogelator can be considered independent of the concentration of precursor and the gelation of precursor can be neglected. It is reasonable to think when this approximation represents less accurately the gelation mechanism, we would obtain less accurate fittings of the hydrolysis/gelation process Since however our scope here is to use relatively simple arguments to understand the source of the different cytotoxicities of the three different stereoisomers, the level of accuracy of the fittings in Figure S12 is entirely within our desired tolerance.

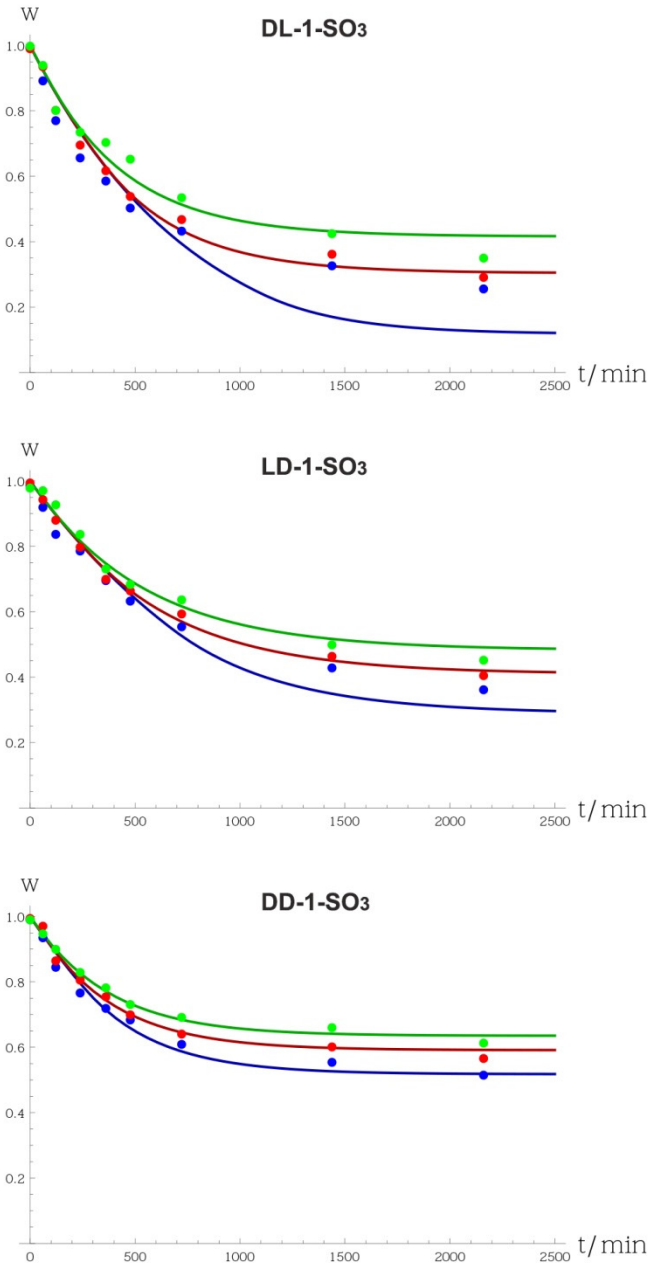


**Figure S12.** Measured (dots) and fitted (lines) time series for the hydrolysis experiments in the absence of tumor cells, for three different values of $S_0$: 100 μM (blue), 200 μM (red) and 500 μM (green). The top plot refers to the DL-**1**-$SO_3$ stereoisomer, the center one to the LD-**1**-$SO_3$ and the bottom one to the DD-**1**-$SO_3$.

### 3.3.3 Transmembrane transport (Group 2)

The group 2 parameters are associated with the transport of precursor across the cell membrane and with the overall velocity of reaction within each compartment (controlled by the concentration of enzyme). In order to obtain experimental time series that are representative of

these processes alone, we performed experiments in conditions under which the population of cells can reasonably be considered as a constant. To reduce population changes due to cell doubling we limited our measures to shorter times (1, 2, 4, 8 and 12 hours) than the doubling time (1 day). In order to limit the amount of cell death due to the action of the drug, we used a moderate initial concentration of precursor (100 μM). Under these conditions we can assume c = c(0) = 1 and neglect the terms in the model associated to cell doubling or death, so that the equations describing this system are:

$$\frac{dw^M}{dt} = -\frac{\delta^M k_{cat} s^M}{K_M + S_0 s^M} - \frac{C_0}{1-C_0}(k_{in} s^M - k_{out} s^C) \tag{71}$$

$$\frac{dy^M}{dt} = +\frac{\delta^M k_{cat} s^M}{K_M + S_0 s^M} \tag{72}$$

$$\frac{dy^C}{dt} = +\frac{\delta^C k_{cat} s^C}{K_M + S_0 s^C} \tag{73}$$

$$\frac{ds^M}{dt} = -\frac{\delta^M k_{cat} s^M}{K_M + S_0 s^M} - \zeta k_g (p^M - K_{gs}^{-1}\Gamma(g^M)) - \frac{C_0}{1-C_0}(k_{in} s^M - k_{out} s^C) \tag{74}$$

$$\frac{dp^M}{dt} = +\frac{\delta^M k_{cat} s^M}{K_M + S_0 s^M} - k_g (p^M - K_{gs}^{-1}\Gamma(g^M)) \tag{75}$$

$$\frac{dg^M}{dt} = +k_g (p^M - K_{gs}^{-1}\Gamma(g^M)) \tag{76}$$

$$\frac{ds^C}{dt} = -\frac{\delta^C k_{cat} s^C}{K_M + S_0 s^C} + k_{in} s^M - k_{out} s^C \tag{77}$$

$$\frac{dp^C}{dt} = +\frac{\delta^C k_{cat} s^C}{K_M + S_0 s^C} - k_g (p^C - K_{gs}^{-1}\Gamma(g^C)) \tag{78}$$

$$\frac{dg^C}{dt} = +k_g (p^C - K_{gs}^{-1}\Gamma(g^C)) \tag{79}$$

The values of $\delta^M$ and $\delta^C$ only depend on the intracellular and extracellular concentrations of enzyme and are therefore the same for all the three datasets relative to the three stereoisomers. As for the transport rate constant $k_{in}$ and $k_{out}$, since we didn't assume any active transport by the cell membrane we have no valid reason to think that they should be different for the three different stereoisomers: in the absence of some sort of active chemical recognition by the membrane, the three stereoisomers have the same physical properties with regard to the transport

process (same mass, same average velocity, same volume, etc) because they are essentially the very same molecules but whose groups are oriented in different directions. We therefore assume that the values of all the parameters at group 2 are the common to the three stereoisomers. As a consequence, we fit them on all the datasets relative to the different stereoisomers at the same time. What we can measure experimentally are the total concentrations of precursor and hydrogelator inside and outside the cells at different times. We therefore performed the fitting by numerically integrating the system of equations (71)-(79) and then fit the values of $w^M$, $y^M$, $s^C$ and $y^C$ at the same time. In other words, the fitting have been performed in a multivariate fashion considering the time, the chemical species and the stereoisomer type as independent variables. Figure S13 shows the outcome of the fitting, while the values of $\delta^M$, $\delta^C$, $k_{in}$, and $k_{out}$ are reported in Table 1. As it can be seen from picture S13, the fitted curves are in good quantitative agreement with the experimental points.

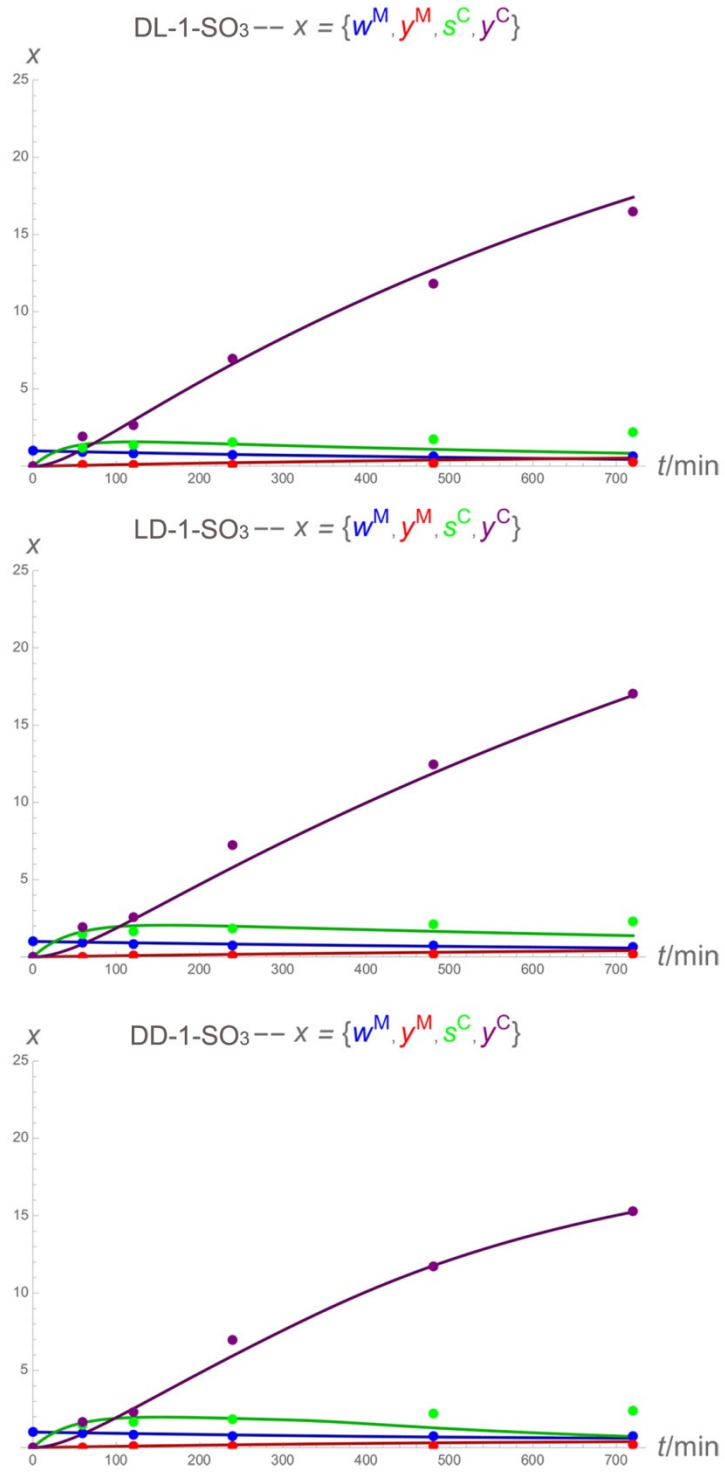


**Figure S13.** Measured (dots) and fitted (lines) time series for the short-times transport experiments starting with an initial concentration of 100 µM. The different colors refer to different variables: $w^M$ (blue), $y^M$ (red), $s^C$ (green) and $y^C$ (purple). The top plot refers to the DL-**1**-$SO_3$ stereoisomer, the center one to the LD-**1**-$SO_3$ and the bottom one to the DD-**1**-$SO_3$.

### 3.3.4 Cytotoxicity (Group 3)

Finally the only parameters left to fit are those relative to the cytotoxicity of the three gels, or in other words the three quantities $k_k^0$ , σ and $[G^C]_{tr}$ characterizing the killing rate constant functional (34). In order to fit these quantities we place the tumor cells in solutions at different initial concentrations of precursor – 20, 50, 100, 200 and 500 μM - and we measure the cell viability after 12, 24, 48 and 72 hours of incubation. The cell viability ρ is calculated as the ratio between the number of live tumor cells in the test solution at a certain time divided by the number of cells in a fresh culture medium (control group) at the same time. The fresh culture medium in control group has the same volume and the same initial number of cells as the test solution, but it contains no precursor. If we call $c^{ctrl}$ the adimensional concentration of cells in the control system, we can define the cell viability as

$$\rho = \frac{c}{c^{ctrl}} \tag{80}$$

Given that the dynamics of control system is fully described by the evolution equation

$$\frac{dc^{ctrl}}{dt} = k_d c^{ctrl} \tag{81}$$

While the evolution equation for the cells in the test system reads - see equation (57) -

$$\frac{dc}{dt} = (k_d - k_k(S_0 g^C))c \tag{82}$$

We can derive an explicit differential equation for the time evolution of ρ:

$$\frac{d\rho}{dt} = -k_k(S_0 g^C)\rho \tag{83}$$

Equation (83) together with equations (54)-(60) and (34) - which for convenience reasons we re-write hereafter - fully describe the dynamics of our system:

$$k_k(S_0 g^C) = \frac{k_k^0}{2}(1 + \tanh(2\sigma(S_0 g^C - [G^C]_{tr}))) \tag{84}$$

$$\frac{d\rho}{dt} = -k_k(S_0 g^C)\rho \tag{85}$$

$$\frac{dc}{dt} = (k_d - k_k(S_0 g^C))c \tag{86}$$

$$\frac{ds^M}{dt} = -\frac{\delta^M \rho\% k_{cat} s^M}{K_M + S_0 s^M} - \zeta k_g (p^M - K_{gs}^{-1}\Gamma(g^M)) - \frac{C_0 c}{1 - C_0 c}(k_{in} s^M - k_{out} s^C)$$

$$+ \frac{C_0 c}{1 - C_0 c}(k_d s^M - k_k (S_0 g^C)(s^M - s^C)) \quad (87)$$

$$\frac{dp^M}{dt} = +\frac{\delta^M \rho\% k_{cat} s^M}{K_M + S_0 s^M} - k_g (p^M - K_{gs}^{-1}\Gamma(g^M)) + \frac{C_0 c}{1 - C_0 c}(k_d p^M - k_k (S_0 g^C)(p^M - p^C)) \quad (88)$$

$$\frac{dg^M}{dt} = +k_g (p^M - K_{gs}^{-1}\Gamma(g^M)) + \frac{C_0 c}{1 - C_0 c}(k_d - k_k (S_0 g^C)) g^M \quad (89)$$

$$\frac{ds^C}{dt} = -\frac{\delta^C \rho\% k_{cat} s^C}{K_M + S_0 s^C} + k_{in} s^M - k_{out} s^C - k_d s^C \quad (90)$$

$$\frac{dp^C}{dt} = +\frac{\delta^C \rho\% k_{cat} s^C}{K_M + S_0 s^C} - k_g (p^C - K_{gs}^{-1}\Gamma(g^C)) - k_d p^C \quad (91)$$

$$\frac{dg^C}{dt} = +k_g (p^C - K_{gs}^{-1}\Gamma(g^C)) - k_d g^C \quad (92)$$

In order to fit the values of $k_k^0$, σ, and $[G^C]_{tr}$ we numerically integrate the systems of equations (84)-(92) and fit the value of ρ on the experimentally measured viability data at different times. Since the gel structure and interaction with the cell is different for each stereoisomer, we perform three separate fittings for the three stereoisomers. For each stereoisomer, we fit the time series of ρ for the different $S_0$ values at the same time, so that again we have an effectively multivariate fitting where t and $S_0$ play the role of independent variables. Figures S14 and 7 show the outcome of the fittings, while the values of $k_k^0$, σ, and $[G^C]_{tr}$ are reported in Table 1. By looking at the top row of plots in Figure S14, we can see that the model is quite successful in reproducing the trend of the experimental data.

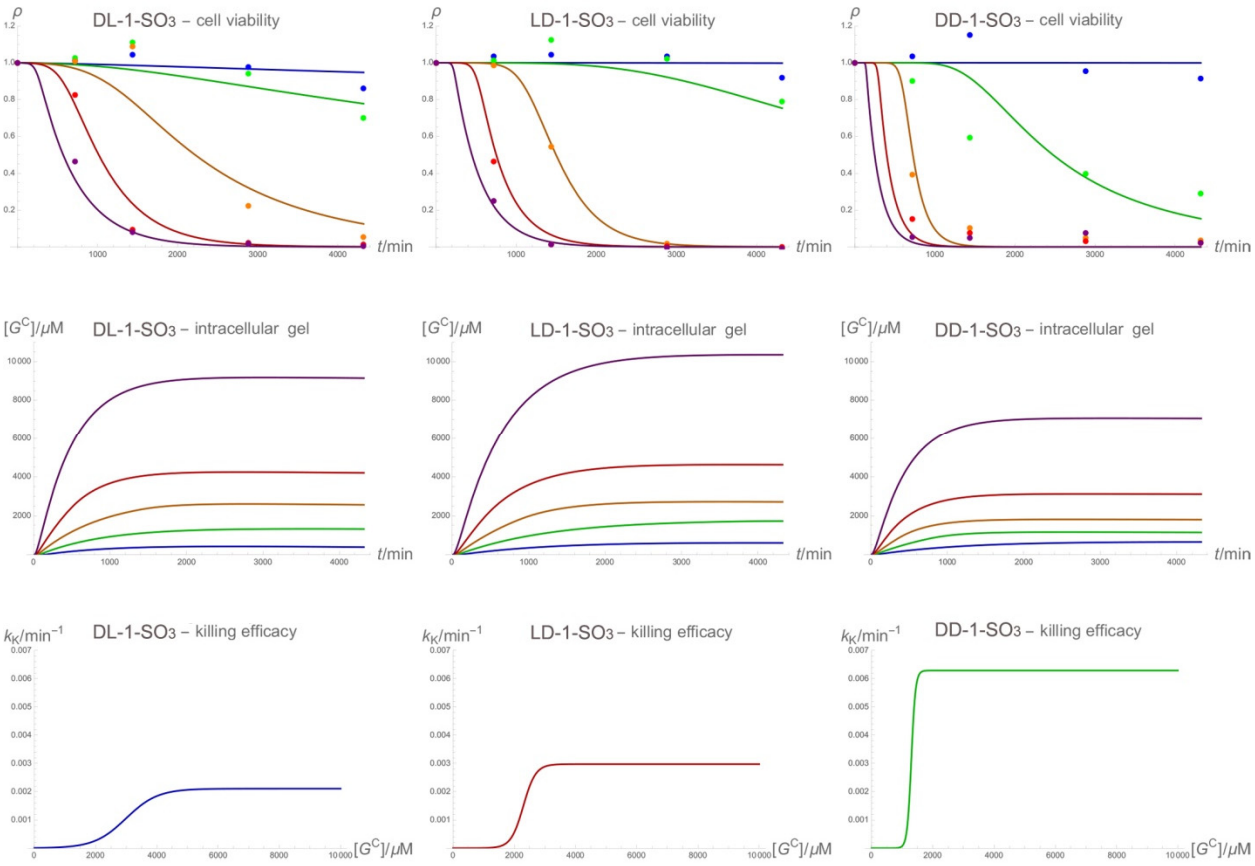


**Figure S14** cell viability fittings for the DL-**1**-$SO_3$ (left column), LD-**1**-$SO_3$ (center column) and DD-**1**-$SO_3$ (right column). The top row shows the experimentally measured values of the cell viability (points) and the fitted values of ρ calculated with model (100)-(108) (lines) for different values of $S_0$: 20 μM (blue), 50 μM (green), 100 μM (orange), 200 μM (red) and 500 μM (purple). The center row shows the intracellular gel concentration as a function of time predicted by the model for the different values of $S_0$ (color coding is the same as top row). The bottom row shows the values of the killing rate constants of the three stereoisomers DL-**1**-$SO_3$ (dark blue), LD-**1**-$SO_3$ (dark red) and DD-**1**-$SO_3$ (dark green) as a function of the intracellular gel concentration $[G^C]$.